Eicosapentaenoic acid induces DNA demethylation in carcinoma cells through a TET1-dependent mechanism

Veronica Ceccarelli,* Virginia Valentini,[†] Simona Ronchetti,[‡] Lorenza Cannarile,[‡] Monia Billi,* Carlo Riccardi,[‡] Laura Ottini,[†] Vincenzo Nicola Talesa,* Francesco Grignani,* and Alba Vecchini*[,1]
*Department of Experimental Medicine and [‡]Department of Medicine, University of Perugia, Perugia, Italy; and [†]Department of Molecular Medicine, Sapienza University, Rome, Italy

ABSTRACT: In cancer cells, global genomic hypomethylation is found together with localized hypermethylation of CpG islands within the promoters and regulatory regions of silenced tumor suppressor genes. Demethylating agents may reverse hypermethylation, thus promoting gene re-expression. Unfortunately, demethylating strategies are not efficient in solid tumor cells. DNA demethylation is mediated by ten-eleven translocation enzymes (TETs). They sequentially convert 5-methylcytosine (5mC) to 5-hydroxymethylcytosine (5hmC), which is associated with active transcription; 5-formylcytosine; and finally, 5-carboxylcytosine. Although α-linolenic acid, eicosapentaenoic acid (EPA), and docosahexaenoic acid, the major n-3 polyunsaturated fatty acids, have anti-cancer effects, their action, as DNA-demethylating agents, has never been investigated in solid tumor cells. Here, we report that EPA demethylates DNA in hepatocarcinoma cells. EPA rapidly increases 5hmC on DNA, inducing p21$^{\text{Waf1/Cip1}}$ gene expression, which slows cancer cell-cycle progression. We show that the underlying molecular mechanism involves TET1. EPA simultaneously binds peroxisome proliferator-activated receptor γ (PPARγ) and retinoid X receptor α (RXRα), thus promoting their heterodimer and inducing a PPARγ−TET1 interaction. They generate a TET1-PPARγ-RXRα protein complex, which binds to a hypermethylated CpG island on the p21 gene, where TET1 converts 5mC to 5hmC. In an apparent shuttling motion, PPARγ and RXRα leave the DNA, whereas TET1 associates stably. Overall, EPA directly regulates DNA methylation levels, permitting TET1 to exert its anti-tumoral function.—Ceccarelli, V., Valentini, V., Ronchetti, S., Cannarile, L., Billi, M., Riccardi, C., Ottini, L., Talesa, V. N., Grignani, F., Vecchini, A., Eicosapentaenoic acid induces DNA demethylation in carcinoma cells through a TET1-dependent mechanism. FASEB J. 32, 000–000 (2018). www.fasebj.org

KEY WORDS: 5-hydroxymethylcytosine · polyunsaturated fatty acids · PPARγ · RXRα

DNA methylation, a widely studied epigenetic modification, plays major roles in genomic stability, X-chromosome inactivation, chromatin accessibility, nucleosome positioning, and gene expression (1, 2). During methylation, DNA methyltransferases (DNMTs) catalyze a covalent chemical reaction that adds a methyl group to the cytosine ring carbon 5 position in CpG dinucleotides.

In most cancer cells, DNA methylation is characterized by global genomic hypomethylation and regional hypermethylation (3, 4). Global hypomethylation may activate oncogenes and retrotransposons, imprinting loss and chromosomal instability (5). On the other hand, regional hypermethylation, at gene promoter and regulatory regions on CpG islands, is one of the major mechanisms for silencing tumor-related genes. DNA hypermethylation is reversible, as demethylating agents can promote re-expression of tumor suppressor genes (6). Although demethylating agents, such as 5-azacytidine and 5-aza-2′-deoxycytidine (5-aza), are approved for therapeutic use in some leukemic syndromes (7), demethylating strategies are not particularly effective in solid tumor cells (8). Consequently, the discovery of demethylating molecules that are active in hepatocarcinoma cells (HCCs) could impact greatly on epigenetic therapy (9).

Recent evidence showed that ten-eleven translocation enzyme (TET) proteins mediate active DNA demethylation (10). Each TET family member (TET1, TET2, and TET3)

is an oxoglutarate- and iron-dependent dioxygenase that catalyses 5-methylcytosine (5mC) oxidation to generate 5-hydroxymethylcytosine (5hmC) (11), which is associated with active transcription (12). Sequential 5hmC oxidation generates 5-formylcytosine and 5-carboxylcytosine (13), both of which may be removed by thymine DNA glycosylase. Alternatively, active DNA demethylation may be promoted by 5hmC deamination, followed by base-excision repair. In fact, TET protein dysregulation and 5hmC loss could lead to carcinogenesis (14, 15).

In the human body, n-3 polyunsaturated fatty acids (PUFAs) are primarily obtained from dietary sources (16), as eicosapentaenoic acid (EPA) and docosahexaenoic acid, 2 major n-3 PUFAs, are weakly synthesized from α-linolenic acid (17). n-3 PUFAs have anti-cancer effects, which are mainly related to modulation of membrane-associated signal transduction, gene expression in cancer pathogenesis, and systemic inflammation (18, 19). Moreover, n-3 PUFA eicosanoid derivatives, such as prostaglandin (PG)E3 and other 3-series PGs, exhibit anti-proliferative and anti-inflammatory activities that slow tumor development (20, 21). PGE3 and other eicosanoid metabolites were recognized as biomarkers that could potentially mediate EPA anti-cancer activity (22).

The present study follows our previous work, which reported that EPA acted as a DNA demethylating agent in leukemia cells (23, 24). Here, we explored in solid cancer cells the molecular mechanism underlying EPA-related DNA demethylation, an as-yet uninvestigated field. In HCCs, we found that specific EPA binding to both peroxisome proliferator-activated receptor γ (PPARγ) and retinoid X receptor α (RXRα) was the starting point for inducing p21 expression, which then inhibited cancer cell-cycle progression. In binding simultaneously to PPARγ and RXRα, EPA assembled the TET1-PPARγ-RXRα protein complex, which reached DNA. There, TET1 induced DNA demethylation by enriching 5hmC in an exonic CpG island, which, in turn, induced p21 gene transcription. TET1 remained bound to DNA, whereas PPARγ and RXRα exited. These results exclude involvement of eicosanoid derivatives and establish that EPA itself functions as a ligand for both receptors.

MATERIALS AND METHODS

Materials

Oleic acid (OA; 18:1, *n*-9), EPA (20:5, n-3), bovine serum albumin (BSA) fraction V (fatty acid free), and 5-aza were purchased from MilliporeSigma (Burlington, MA, USA).

Albumin-bound fatty acids

A stock solution of each fatty acid (5 or 10 mM) was prepared, as previously described (23). In brief, free fatty acid was diluted in ethanol and precipitated by adding NaOH (final concentration: 0.25 M). The precipitate was dried under nitrogen, reconstituted with 0.9% (w/v) NaCl, and stirred at room temperature for 10 min with defatted BSA fraction V fatty acid free (final

concentration: 10% w/v) in 0.15 M NaCl. Each solution was adjusted to pH 7.4 with NaOH and stored in the dark in aliquots at $-20°C$ under nitrogen. The fatty acid/BSA molar ratio was 4:1.

Cell culture and treatments

The rat hepatoma cell line McRH-7777 (CRL-1601) from American Type Culture Collection (Manassas, VA, USA) was cultured in DMEM and supplemented with 20% horse serum, 5% fetal calf serum, 2 mM L-glutamine, and 1% penicillin/streptomycin at 37°C in a humidified incubator, aerated with 5% CO_2. Cells were seeded at a density of 0.3×10^6 cells/ml for all experiments. Cells were incubated with fatty acid/BSA solutions and 5-aza at the indicated concentrations and times.

Cell cycle and viability

RH-7777 cells were treated with 100 μM fatty acids and 1 μM 5-aza for 3, 24, and 48 h and analyzed by flow cytometry. After washing and centrifuge at 200 g, cell pellets were resuspended in 1 ml hypotonic propidium iodide (PI) solution (50 μg/ml^{-1} in 1% sodium citrate plus 0.1% Triton X-100; MilliporeSigma). Samples were placed overnight in the dark at 4°C. The PI fluorescence of individual nuclei was measured using an EPICS XL-MCL flow cytometer (Beckman Coulter, Miami, FL, USA). The cell cycle was analyzed by measurement of DNA-bound PI fluorescence in the orange-red fluorescence channel (FL2) through a 585/42 nm bandpass filter with linear amplification. Distribution profiles were analyzed using ModFit LT software (Verity Software House, Topsham, ME, USA) to determine cell fractions in each phase of the cell cycle (G_0/G_1, S, G_2/M). At least 15,000 events were collected for each sample. Cells were gated on FL2-area *vs.* FL2-width plots to exclude aggregates and debris (25). Cell viability after 3, 24, and 48 h fatty acid treatments was determined by counting triplicate samples for Trypan blue dye-excluding cells.

Quantitative RT-PCR

Total RNA was extracted from control cells and after 3-, 24-, and 48-h treatments with 100 μM fatty acids and 1 μM 5-aza using the Trizol reagent (Invitrogen S.r.l., Milano, Italy), according to the manufacturer's guidelines. Reverse transcription was performed using the Quanti Tect Reverse Transcription Kit (Qiagen, Hilden, Germany). Quantitative RT-PCR (qRT-PCR) was performed using the Mx3000P Real-Time PCR System with brilliant SYBR Green qPCR Master Mix (Stratagene, San Diego, CA, USA) and Rox as reference dye. qRT-PCR reactions were performed under standardized conditions for each primer set.

Each time point was investigated with 4 replicates of 3 independent experiments for p21 (NM_080782 mRNA). The primers were the following: forward, 5′-AGTATGC-CGTCGTCTGTTC-3′; reverse, 5′-CAAAGTTCCACCGTTC-TCG-3′. Rat hypoxanthine-guanine phosphoribosyltransferase mRNA was the housekeeping gene. The $\Delta\Delta C_t$ method determined mRNA modulation (23).

Immunoblot analysis

RH-7777 cells were cultured in standard conditions with 100 μM fatty acids or 1 μM 5-aza for 3, 24, and 48 h. Protein samples (70 μg) from total cell lysates were subjected to SDS-PAGE, electroblotted onto a nitrocellulose membrane (Schleicher and Schuell, Keene, NH, USA), and probed with the following antibodies: anti-p21, sc-6246 (Santa Cruz Biotechnology, Dallas, TX, USA);

anti-TET1, sc-163446 (Santa Cruz Biotechnology); anti-TET2, ab123816 (Abcam, Cambridge, MA, USA); anti-TET3, PA5-34431 (Pierce, Dallas, TX, USA); anti-PPARγ, PA3-821A (Thermo Fisher Scientific, Waltham, MA, USA); and anti-RXRα, ab28767 (Abcam). Immunoreactive bands were visualized using the ECL assay (Amersham Pharmacia Biotech, Little Chalfont, United Kingdom). Anti-β-Tubulin antibody (MilliporeSigma) was used to normalize. Images were acquired using the VersaDoc Imaging System (Bio-Rad, Hercules, CA, USA), and signals were quantified using Quantity One software (Bio-Rad).

DNA isolation and p21 CpG island quantitative DNA methylation

Genomic DNA from control RH-7777 cells or 100 μM OA or EPA cells after 24 h treatment was extracted using FlexiGene DNA Kit (Qiagen). European Molecular Biology Open Software Suite (*http://emboss.sourceforge.net/*) and MethPrimer (*http://www.urogene.org/methprimer/*) online software programs were used to identify potential CpG islands for the p21 gene. DNA methylation levels were quantified for rat p21 (MePH25981-3A; Qiagen) using the Methyl-Profiler qPCR Primer Assay. Primers were designed by an optimized computer algorithm to ensure that the amplicon contained cutting sites for both methyl-sensitive and -dependent enzymes. The qRT-PCR program was performed as instructed. DNA methylation status of CpG islands was determined using restriction enzyme digestion (DNA Methylation Enzyme Kit MeA-03; Qiagen), followed by SYBR Green-based qRT-PCR detection, as previously described (23). The relative amount of each DNA fraction (methylated and unmethylated) was calculated using the ΔC_t method (23).

Bisulfite modification of genomic DNA and sequencing

With the use of the FlexiGene DNA Kit (Qiagen), genomic DNA was obtained from RH-7777, control, or after 3, 24, and 48 h treatment with 100 μM OA and EPA. The bisulfite reaction to determine DNA methylation status was performed, as previously described (26). DNA fragments covering p21 CpG island V (8021/8241) were amplified by PCR using the following primers: forward, 5′-TTTGTGTTTTAGTTATAGGTATTATGTT-3′; reverse, 5′-AAATCTTAAACAACCCTAAACTCC-3′. The PCR products were cloned into pCR2.1 TOPO (Invitrogen S.r.l.), and 7 randomly picked clones from each of 2 independent PCRs were sequenced using T7 primer at the Genechron-Ylichron Laboratory (Rome, Italy).

Methylation-specific DNA pyrosequencing analysis

DNA from RH-7777 cells was extracted using the FlexiGene Kit (Qiagen), following the manufacturer's instructions. DNA bisulfite modification was performed using the EpiTect Plus DNA Bisulfite Kit (Qiagen), according to the manufacturer's instructions. CpG island methylation, at a total of 163 CpG sites within p21 intron 1 and exon 2, was analyzed in untreated controls and cells that had been treated with 100 μM OA and EPA or 1 μM 5-aza, for 3, 24, and 48 h. Methylation was quantified by pyrosequencing, a highly sensitive and reproducible method that provides information for each CpG site, using the PyroMark Q24 (Qiagen) platform. Specific primers (Supplemental Table 1) were designed using Pyromark Assay Design Software, v.2 (Qiagen) to analyze the 5 p21 gene CpG islands. A standard pyrosequencing sample preparation protocol was applied (27). Methylation at each CpG site was determined from the C→T ratio by Pyromark Q24

Software (Qiagen). Methylation for each p21 island was expressed as the mean percentage at all CpG sites.

Dot blot

Isolated DNA (1 μg/sample) was denatured in 0.1 M NaOH for 10 min at 95°C and neutralized with 0.1 vol NH$_4$ acetate 6.6 M on ice. DNA samples were spotted on a Hybond N$^+$ nylon membrane (GE Healthcare, Little Chalfont, United Kingdom) using a Bio-Dot apparatus (Bio-Rad). The membrane was cross-linked at 120°C for 30 min and blocked by 5% nonfat milk for 1 h at room temperature. It was then incubated overnight at 4°C in 0.2 μg/ml rabbit polyclonal anti-5hmC: 39791 (Active Motif, Carlsbad, CA, USA), or 0.5 μg/ml mouse monoclonal anti-5mC: 61479 (Active Motif). The blotted membrane was washed 3 × 10 min in Tris-buffered saline (TBS) + 0.1% Tween-20 and then incubated for 1 h at room temperature with horseradish peroxidase-conjugated goat anti-rabbit IgG (MilliporeSigma, Burlington, MA, USA) or with horseradish peroxidase-conjugated goat anti-mouse IgG (Thermo Fisher Scientific) secondary antibodies in TBS + 0.1% Tween-20. The membrane was then washed 3 × 10 min in TBS + 0.1% Tween-20 and visualized by chemiluminescence with the SuperSignal West Dura Extended Duration Substrate (Pierce). The equal-loading amount of total DNA on the membrane was confirmed by staining with 0.02% methylene blue in 0.03 M sodium acetate (pH 5.2).

Hydroxymethylated DNA immunoprecipitation and methylated DNA immunoprecipitation assays

Fragmented DNA (0.5 μg/sample; 200–1000 bp in size) was denatured for 10 min at 95°C. The hydroxymethylated DNA immunoprecipitation (hMeDIP; P-1038-24; Epigentek, Farmingdale, NY, USA) and methylated DNA immunoprecipitation (MeDIP; P-2019-24; Epigentek) assays were performed, according to the manufacturer's instructions. Antibody buffer (100 μl) was added to the following antibodies: 1 μl nonimmune IgG (negative controls), 1 μl anti-5hmC, and 1 μl anti-5mC, and incubated at room temperature for 60 min. After removing the antibody buffer from the wells and washing with diluted washing buffer, 0.5 μg fragmented DNA was added to each well. After incubation for 90 min at room temperature on an orbital shaker, the reaction wells were washed with diluted washing buffer. Proteinase K was added for 15 min at 60°C, and the reaction wells were incubated at 95°C for 3 min to inactivate the enzyme. DNA samples were subject to qRT-PCR using Brilliant SYBR Green qPCR Master Mix. The following primers were used to amplify the island V sequence: forward, 5′-CCCGGAACTG-GAAGATTGT-3′; reverse, 5′-AGGTACTGGGCCTCTTGTCC-3′. Fold enrichment was calculated by means of the amplification efficiency ratio of hMeDIP or MeDIP DNA samples over nonimmune IgG by using $2^{\Delta(\text{IgG } Ct - \text{ sample } Ct)}$.

Chromatin immunoprecipitation (ChIP)

Using the EZ-ChIP Kit (MilliporeSigma), ChIP assays were performed on ~20 × 10^6 RH-7777 cells or after 100 μM OA or EPA treatment for 3, 24, and 48 h. Cells were crosslinked and cell lysates sonicated until chromatin fragments became 200–1000 bp in size. Mouse RNA polymerase II (RNAPII) 8WG16 mAb MMS-126R (Covance, Princeton, NJ, USA), rabbit TET1 09-872 (MilliporeSigma), goat TET2 ab123816 (Abcam), rabbit TET3 PA5-34431 (Pierce), mouse PPARγ antibody (Abcam), and mouse RXRα sc-2553 (Santa Cruz Biotechnology) were used for immunoprecipitation (IP). Mouse IgG (Thermo Fischer Scientific), rabbit IgG (MilliporeSigma), and goat IgG (Santa Cruz Biotechnology) were

used as negative controls. After IP, recovered chromatin samples were subjected to qRT-PCR with Brilliant SYBR Green qPCR Master Mix. The following primers were used: forward, 5′-CCCGGAACTGGAAGATTGT-3′; reverse, 5′-AGGTACTGG-GCCTCTTGTCC-3′. Data were analyzed quantitatively according to the formula $2^{-\Delta[Ct(IP) - Ct(input)]} - 2^{-\Delta[Ct(control\ IgG) - Ct(input)]}$ (28).

PPAR response element

Island V was analyzed for PPAR response element (PPRE) or its variants using Dragon PPAR Response Element Spotted v.2.0 (Computational Bioscience Research Centre, Thuwal, Saudi Arabia).

Co-IP assay

Nuclear extracts were prepared from RH-7777 cells after 24 h EPA conditioning and were diluted with IP buffer (50 mM Tris-HCl, pH 8), 100 mM NaCl, 5 mM MgCl$_2$, and 0.2% Nonidet P-40. After incubation with Dynabeads Protein A (Thermo Fisher Scientific), anti-PPARγ PA3-820 (Thermo Fisher Scientific) was added to the diluted nuclear extract. After overnight incubation, the beads were washed with IP buffer, and IP proteins were analyzed by Western blotting. The antibodies were the following: PPARγ PA3-821A (Thermo Fisher Scientific), TET1 sc-163446 (Santa Cruz Biotechnology), and RXRα ab28767 (Abcam). PPARγ (5 μg) was used per IP.

Immunofluorescence

Cell controls (2×10^5) and cells after 3, 24, and 48 h treatment with 100 μM OA and EPA were cytospun for 4 min at 400 rpm, rinsed with ice-cold PBS, and fixed with 4% paraformaldehyde for 20 min at room temperature, followed by 1 h incubation with blocking buffer (0.1% Triton X-100, BSA 3% in PBS). The cells were subjected to immunofluorescence staining with mouse 5hmC HMC/4D9 (Epigentek; 1:300). Immunofluorescence for 5mC was performed as follows: after fixation with 4% para-formaldehyde for 10 min, cells were permeabilized with 0.5% Triton X-100 for 1 h and treated with 2 N HCl for 45 min at room temperature. After blocking with PBS containing 0.1% Triton X-100 and 1% BSA for 1 h, cells were incubated overnight at 4°C with mouse 5mC 33D3 (Epigentek; 1:500) antibody. Cells were then washed with cold PBS, 3 times for 3 min each, and incubated at room temperature for 1 h with Alexa Fluor 488-labeled anti-mouse secondary antibody (1:100; Thermo Fisher Scientific). Nuclei were counterstained with DAPI (MilliporeSigma). Cell fluorescence was analyzed using a Zeiss Axioplan fluorescence microscope equipped with a Spot-2 cooled camera (Diagnostic Instruments, Sterling Heights, MI, USA). Positive stained nuclei were counted, and 10 fields from each experimental condition were quantified and statistically analyzed using the Student's t test. Statistical significance was accepted when $P < 0.05$. Values are presented as means ± SD.

5hmC immunofluorescence analysis, using dimethyloxallyl glycine (DMOG; MilliporeSigma), investigated TET protein inhibition. Cells were cultured in DMEM complete medium and treated for 4 h with 1 mM DMOG diluted in PBS buffer. After DMOG, another sample was treated with 100 μM EPA for 3 h.

Proximity ligation assays

Cells (2×10^5 cells) were cytospun for 4 min at 400 rpm, rinsed with ice-cold PBS, fixed with 4% paraformaldehyde for 20 min at room temperature, and blocked with blocking buffer (0.1% Triton X-100, BSA 3% in PBS) for 1 h at room temperature, which also permeabilized the cells. Slides were immunostained at 4°C overnight with the following primary antibodies: goat anti-TET1 sc-163446 (Santa Cruz Biotechnology; 1:500), rabbit anti-PPARγ PA3-821A (Thermo Fisher Scientific; 1:200), mouse anti-PPARγ sc-7273 (Santa Cruz Biotechnology; 1:50), rabbit anti-EPA PAO122Ge01 (Cloud-Clone, Houston, TX, USA; 1:100), and goat anti-RXRα ab28767 (Abcam; 1:200). Duolink in situ proximity ligation assay (PLA; MilliporeSigma) was performed, according to the manufacturer's protocol. In brief, PLA probe solution and ligation-ligase solution were added for 1 h and 30 min, respectively. The signal was amplified with amplification-polymerase solution at 37°C for 100 min (Duolink in situ; MilliporeSigma). Nuclei were counterstained with DAPI. Slides were analyzed using the Zeiss Axioplan fluorescence microscope, equipped with a Spot-2 cooled camera (Diagnostic Instruments). Positive-stained nuclei were counted, and 10 fields from each experimental condition were quantified and statistically analyzed using the Student's t test. Statistical significance was accepted when $P < 0.05$. Values are presented as means ± SD.

Statistical analyses

All results are presented as means ± SD and were analyzed by 1-way ANOVA with Bonferroni's post-test. A value of $P < 0.05$ was considered significant.

RESULTS

EPA inhibited cell-cycle progression and cell viability and increased p21 expression in HCCs

As EPA acted as a demethylating agent in leukemia cells (23, 24), we explored its action in several HCC lines. RH-7777 rat HCCs emerged as an efficient experimental model. We determined the effects of EPA on cell-cycle distribution of the cells. After EPA treatment, the G$_0$/G$_1$ phase increased significantly in a concentration- and time-dependent manner (**Fig. 1A, B**). OA, a monoun-saturated fatty acid, had no effect under any of the study conditions, confirming findings in leukemic cells (23) (Fig. 1A, B). In 48 h , EPA conditioning induced 10–15% cell apoptosis and was associated with a significant, time-dependent reduction in cell viability (Fig. 1C). p21$^{Waf1/Cip1}$, a cyclin-dependent kinase inhibitor, is encoded by the *cyclin-dependent kinase N1A* gene, expression of which is inversely related to cell-cycle progression (29). As decreased p21 expression leads to excessive cell proliferation and cell-cycle dysregulation in HCC (30), we examined p21 mRNA and protein levels after conditioning with EPA, OA, and 5-aza, a well-known DNA-demethylating agent (Fig. 1D–F). In 24 and 48 h, 5-aza treatment increased p21 mRNA and protein expression. Surprisingly, 3 h EPA treatment significantly increased p21 mRNA and protein expression, which remained constantly high for up to 48 h. 5-aza and EPA treatments seemed to act by different transcription processes, as the kinetic profiles of p21 mRNA and protein were similar (Fig. 1D, F). These findings indicated that EPA and 5-aza decreased RH-7777 cell proliferation and induced p21 expression. The very early EPA-induced increase in p21 expression was the first

Figure 1. Effects of EPA on RH-7777 cell-cycle, viability, and p21 expression. *A*) G_0/G_1 cell-cycle distribution. Flow cytometry of RH-7777 cells after 24 h treatment with OA ($\triangle$) and EPA ($\bigcirc$). Means $\pm$ sd of 5 experiments are shown (*$P < 0.01$). *B*) Cell-cycle distribution phases. Cells were treated with 100 µM fatty acids for 24 h. One of 5 experiments is shown as representative. *C*) Effects of 100 µM fatty acid treatments on cell proliferation. Controls (white bars), OA (gray bars), and EPA (black bars). Means $\pm$ sd of 5 experiments are shown (*$P < 0.01$). *D*) qRT-PCR shows p21 mRNA content in controls (white bars), OA (light gray bars), EPA (black bars), and 5-aza (dark gray bars) after 100 µM fatty acids and 1 µM 5-aza. Means $\pm$ sd of 3 experiments are shown (*$P < 0.05$). *E*) Western blot analysis for p21 in controls (C) and after 100 µM OA and EPA and 1 µM 5-aza. One of 4 experiments is reported as representative. *F*) Western blot band density *vs.* untreated controls. Controls (white bars), OA (light gray bars), EPA (black bars), and 5-aza (dark gray bars). Data are the means $\pm$ sd of 4 experiments (*$P < 0.05$).

step in transcription. It might have been a result of a specific molecular mechanism, which decreased proliferation and cell-cycle progression later in the 24 h exposure.

Effects of EPA on the p21 gene CpG islands

To support the hypothesis that EPA promoted DNA demethylation, we sought for CpG islands on the p21 gene. The sequence we analyzed (−1000/+8459) contained 1000 bp upstream to the transcription start site, untranslated exon 1, intron 1, and exon 2 (**Fig. 2A**). Five CpG islands were retrieved, hence forward-termed islands I, II, III, IV, and V (Fig. 2A). Islands I–IV spanned intron 1. The island V nucleotide sequence (Fig. 2B) was located in an internal exon 2 region, adjacent to the ATG (Fig. 2A).

Approximately 96% of p21 DNA copies were unmethylated in untreated HCCs. Methylation status did not

change after 24 h OA and EPA conditioning (Fig. 2C). Seemingly, only a minimal part of DNA needs to be methylated to reduce p21 gene expression. Methylation levels for each CpG island (bisulfite-pyrosequencing analysis) showed that in fact, only island V was methylated (Fig. 2D).

Bisulfite sequencing of island V for single, selected, and cultured clones showed that a few random CpGs were demethylated after EPA treatment (Fig. 2E). This weak CpG demethylation could not account for the strong induction of p21 expression.

Interestingly, after EPA treatment, specific primers (Supplemental Table 1) for island V pyrosequencing analysis revealed that 18 CpG dinucleotides had not changed their methylation levels (Fig. 2F, G). As expected, 5-aza conditioning decreased methylation of each CpG in a time-dependent manner (Fig. 2F, G), in parallel with increased p21 expression. Thus, even though EPA increased p21 gene expression, it did not modify methylation on p21 CpG island V.

Figure 2. Effects of EPA on the p21 gene CpG islands. *A*) p21 gene schema (−1000/+8459). I, II, III, IV, and V indicate CpG islands. *B*) Start exon 2 (red) and nucleotide sequence of CpG island V (bold), showing 18 CpG dinucleotides and 2 PPRE variants (underlined). Italics refer to bisulfite sequencing primers and lowercase to ChIP, hMeDIP, and MeDIP primers. *C*) Methyl-Profiler qPCR Primer Assay quantified p21 unmethylated DNA in all islands after 24 h 100 µM fatty acid treatment. Controls (white bar), OA (light gray bar), and EPA (black bar). *D*) Bisulfite pyrosequencing of 5 CpG islands measured methylation in 163 sites in controls. *E*) Island V-methylated (●) and -unmethylated (○) CpGs after bisulfite reaction on each generated clone. *F*) Bisulfite pyrosequencing of each island V CpG after 100 µM OA and EPA and 1 µM 5-aza treatment. Controls (white bars), 3 h (blue bars), 24 h (green bars), and 48 h (red bars). *G*) Bisulfite pyrosequencing showed total methylation of island V. Controls (□) and after 100 µM OA (△) and EPA (○) and 1 µM 5-aza (▽). Unless otherwise stated, results are the means ± SD of 3 experiments.

EPA effects are TET1 dependent

As active cellular proliferation in liver cancer cells was associated with 5hmC loss (31, 32), and EPA slowed cell-cycle progression, we investigated 5hmC levels after EPA conditioning. We chose dot-blot analyses using 5hmC and 5mC antibodies on genomic DNA, as bisulfite-pyrosequencing analysis does not discriminate between 5mC and 5hmC, which both are read as cytosines (33). After 3, 24, and 48 h EPA treatment, 5hmC content markedly increased (**Fig. 3A, B**), as confirmed by immunofluorescence analyses, using the same antibody (Fig. 3C). No change in 5hmC was observed after OA

(Supplemental Fig. 1*A*, B). No significant differences in 5mC emerged after OA or EPA conditioning compared with control cells (Supplemental Fig. 2*A*, B). Thus, EPA increased 5hmC levels in genomic DNA without affecting cellular 5mC. This apparent discrepancy may be a result of the gap between 5hmC and 5mC levels in cells and of low 5mC content in CpG islands compared with cellular 5mC. In some enhancers, promoters, and gene bodies that are in specific functional regions in the genome, such as p21 island V, 5hmC was enriched, suggesting that it played an active role in transcription (12). The EPA-induced increase in 5hmC was restricted to these functional regions (*e.g.*, CpG islands) that
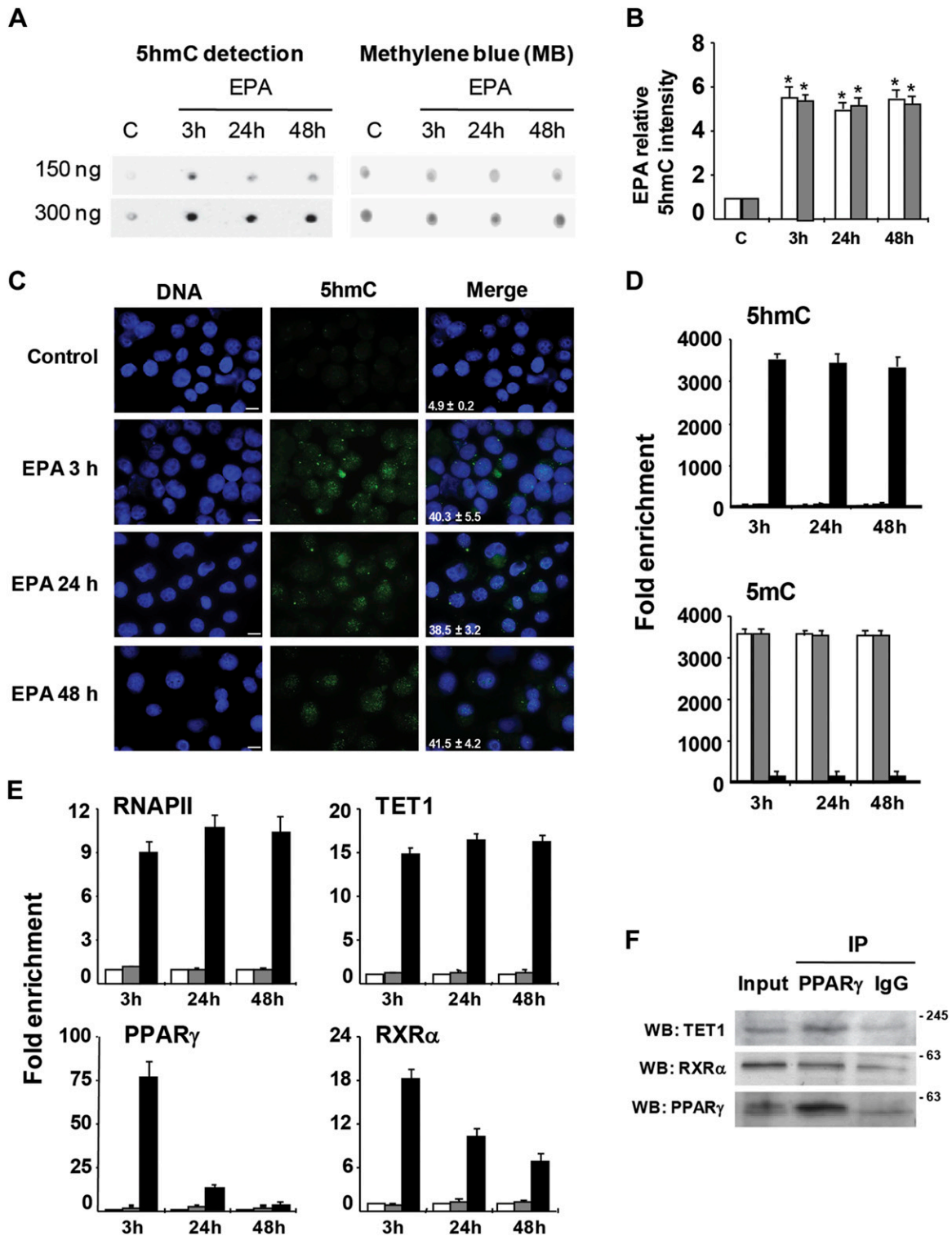
Figure 3. EPA effects are TET1 dependent. *A*) Dot-blot analysis for 5hmC in controls and after 100 μM EPA. *B*) Dot-blot band densities *vs.* controls. (*$P < 0.05$). DNA (150 ng; white bars) and 300 ng DNA (gray bars). *C*) 5hmC immunofluorescence for controls and after EPA. Numbers refer to positive-stained nuclei. Original scale bars, 10 μm. *D*) hMeDIP and MeDIP of island V, using 5hmC and 5mC antibodies. Controls (white bars), OA (gray bars), and EPA (black bars). *E*) Island V ChIP using RNAPII, TET1, PPARγ, and RXRα antibodies and the same primers as the hMeDIP and MeDIP assays. Controls (white bars), OA (gray bars), and EPA (black bars). *F*) PPARγ interacted with TET1 and RXRα. PPARγ was immunoprecipitated using PPARγ antibody from nuclear extract of controls after 3 h EPA. Co-IP TET1 and RXRα were detected by Western blot (WB). Unless otherwise stated, results are the means ± SD of 3 experiments.

constitute specific DNA portions, whereas in total DNA, 5mC was stably conserved. Increased 5hmC levels (Fig. 3A, B) constituted a very small part of the total 5mC, which was distributed across the entire DNA spectrum. To investigate whether 5hmC was present on the p21 island V, we used an hMeDIP assay with the 5hmC antibody. qRT-PCR amplification of island V, containing 18 CpG dinucleotides, was obtained from IP DNA. After 3 h EPA treatment, the hMeDIP assay revealed significant anti-5hmC binding to p21 island V, which remained stable for up to 48 h (Fig. 3D), suggesting that 5hmC has a role to play in p21 expression. The MeDIP assay demonstrated that EPA converted 5mC to 5hmC on island V, in line with the increase in 5hmC binding (Fig. 3D).

We next investigated whether the EPA-induced increase in 5hmC on island V underlay increased p21 expression. ChIP analysis on controls and 3 h after OA and EPA treatments showed significant anti-RNAPII binding to island V, which persisted for up to 48 h, only after EPA treatment (Fig. 3E). 5hmC enrichment overlapped with active p21 transcription, in agreement with increased p21 mRNA and protein levels.

We next investigated whether TET1, TET2, and TET3 proteins (34) were involved in the conversion of 5mC to 5hmC. Western blot analyses found no differences in TET proteins expression after OA and EPA treatments (Supplemental Fig. 3A). In contrast, the ChIP assay, using TET isoform antibodies, detected very high TET1 enrichment on island V of the p21 gene, only after EPA (Fig. 3E). TET2 and TET3 exhibited no detectable binding after OA and EPA (data not shown). TET1 binding persisted for up to 48 h, maintaining a hypomethylated status, which inhibited DNMT activity (35). These data suggest that only the TET1 isoform was involved in increased 5hmC on island V and that EPA induced its activity without affecting its expression. The key role of TET1 activity was further evaluated by immunofluorescence analyses for 5hmC in DMOG-treated cells, as DMOG is a small molecule inhibitor of TET activity. No difference in 5hmC signal levels was observed between control and DMOG-treated cells. After DMOG, EPA treatment did not increase TET1 activity (Supplemental Fig. 3B).

To understand how EPA promoted TET1 binding on island V, we considered the following: 1) fatty acids, such as EPA and fatty acid-derived eicosanoids, are natural PPARγ ligands (36), and 2) PPARγ promotes 5hmC production around the PPRE by recruiting TET1 during adipocyte differentiation (37).

As we had found 2 PPRE variants on island V (Fig. 2B), we performed ChIP analyses using the PPARγ and RXRα antibodies, as both receptors form an active heterodimer after binding with their ligands (38). Interestingly, after 3 h EPA treatment, both displayed significant binding to island V, which gradually dropped at 48 h (Fig. 3E). Western blot analyses showed no differences in PPARγ and RXRα protein levels after EPA treatment (Supplemental Fig. 3). Overall, EPA induced TET1, PPARγ, and RXRα proteins binding to island V of the p21 gene without affecting their expression.

EPA promoted assembly of a TET1-PPARγ-RXRα protein complex

To demonstrate that TET1 physically interacted with PPARγ after 3 h EPA conditioning, we performed a co-IP assay using the PPARγ antibody in a nuclear extract of EPA-treated cells. With the use of TET1 and RXRα antibodies, Western blot analyses showed that both bound PPARγ (Fig. 3F). Thus, a TET1-PPARγ-RXRα protein complex appears to be essential for recruiting TET1 to island V.

The PLA, which investigates direct protein interactions, provided further proof of TET1-PPARγ binding and excluded TET1-RXRα binding after 3 h EPA conditioning. Spots highlighting the TET1-PPARγ interaction decreased within 48 h (**Fig. 4A**), supporting ChIP assay evidence of PPARγ release from island V (Fig. 3E). No spot for TET1-RXRα was found at any time point (Supplemental Fig. 4B), confirming TET1-PPARγ-binding specificity in the co-IP assay. A PLA using PPARγ and RXRα antibodies confirmed that the 2 nuclear receptors formed a heterodimer, interacting physically after 3 h EPA conditioning. Spots dropped in number within 48 h, suggesting heterodimer binding gradually decreased, probably as the bond detached from its ligand (Supplemental Fig. 4A). Fatty acids and their eicosanoid derivatives are natural ligands of PPARγ and RXRα (39, 40). A PLA using the EPA antibody and either the PPARγ or RXRα antibody revealed that EPA bound both PPARγ and RXRα, leading to heterodimer formation. EPA-PPARγ (Fig. 4B) or EPA-RXRα (Fig. 4C) binding was significantly high after 3 h EPA exposure, decreased at 24 h, and disappeared at 48 h. These observations suggested that at 48 h, EPA separates from the 2 receptors, thus breaking up the active heterodimer (**Fig. 5**).

This molecular mechanism coincides with kinetic profiles of PPARγ and RXRα on island V, observed by the ChIP assay, and excludes a role for an EPA eicosanoid metabolic derivative.

DISCUSSION

This study demonstrated that EPA induces DNA demethylation in HCCs. It simultaneously binds PPARγ and RXRα to assemble a TET1-PPARγ-RXRα protein complex, which associates with hypermethylated DNA regions, where TET1 enriches 5hmC. In fact, the ~6-fold 5hmC rise in genomic DNA confirmed that the cells accumulate 5hmC as a stable modification (41). The 5hmC increase on p21 island V, which was observed after 3 h, was the EPA-induced starting change. It enhanced p21 expression, which after 24 h, inhibited cell-cycle progression and cell proliferation. Our observations showed that 5hmC, the first TET1 product in its oxidation chain reaction, remained stable for up to 48 h in DNA. As a consequence, TET1 appeared unable to promote the consecutive oxidation reactions for transforming 5hmC to 5-formylcytosine and 5-carboxylcytosine. No information is, at present, available on the mechanisms of TET1 action when it catalyzes the whole sequential oxidation reactions instead of stably stopping at 5hmC. This crucial topic

Figure 4. PLA showed TET1/PPARγ (*A*), EPA/PPARγ (*B*), and EPA/RXRα (*C*) interactions after EPA. Red spots show a single interaction. DNA counterstaining with DAPI. Merge images show nuclear localization. Original scale bars, 10 μm. Data are the means ± sd of 3 experiments.

requires further investigation in both normal and tumor cells with different phenotypes.

Our results suggest that 5hmC played a functional role in activating transcription. Indeed, we found that in island V, 5hmC rather than 5mC, induced p21 expression in line with the increase in RNAPII binding. Evidence in support of these data derives from experimental models showing that increased 5hmC levels were associated with active transcription (12, 42) and were found on transcription factor-binding sites, enhancers, promoters, and exons in actively expressed genes (43), similar to our findings on the p21 exon 2 island V.

In adipocyte differentiation, the PPARγ-TET1 interaction has previously been reported to produce local 5hmC

Figure 5. Schema of the EPA role in increasing 5hmC in the hypermethylated CpG island V on the p21 gene. *A, B*) EPA simultaneously bound PPARγ and RXRα receptors (*A*) to form their heterodimer and induced a PPARγ-TET1 interaction (*B*). *C*) The TET1-PPARγ-RXRα protein complex bound to the CpG island V on the p21 gene where TET1 converted 5mC to 5hmC. *D*) TET1 associated stably to DNA, whereas PPARγ and RXRα exited, breaking up their heterodimer and EPA binding.

after several days (37). As we found that 5hmC increases within a few hours of EPA treatment, we speculate that molecular mechanisms could vary with cell phenotypes (*i.e.*, adipocytes *vs.* tumor cells). Alternatively, our findings suggest that a simultaneous EPA binding to PPARγ and RXRα might modify the kinetics of the effect, which may be different when EPA binds singularly to PPARγ or RXRα.

As simultaneous binding of both PPARγ and RXRα has never before been described for EPA or other ligands, the possibility exists that other n-3 PUFAs or 3-series eicosanoid derivatives may exhibit a similar action, as they are potential ligands for PPARγ and RXRα (36, 40) and inhibit proliferation in cancer cells with a similar mechanism (20, 21).

Our experiments provided the first evidence that the PPARγ-RXRα heterodimer functioned as a shuttle. It recruited TET1 to island V and then subsequently exited the DNA, leaving TET1 bound to island V (Fig. 5). TET1 maintained the DNA hypomethylated status, probably facilitating gene expression, as previously proposed (35). Indeed, TET1 prefers binding hypomethylated high CpG-dense regions to prevent DNMT activity and inhibit DNA methylation (44).

The increase in 5hmC in the island V p21 gene was likely a result of specific PPARγ-RXRα binding to 2 PPRE variants. Alternatively, the PPARγ-RXRα heterodimer might function simply as a shuttle without binding to the PPRE. To explain the mechanism underlying the increase in 5hmC in whole DNA after EPA treatment, one might speculate that in genome areas different from island V of the p21 gene, where PPREs are not found, PPARγ may bind to other consensus sequences, acting as a monomer or homodimer (45) to recruit TET1.

The increased TET1 activity could be synergistic with TET1 expression upregulation. In fact, as TET1 re-expression opposes cell progression, it is recognized as a tumor-suppressor gene (46). Its downregulation or silencing promoted malignancy and increased cellular proliferation (47) and may be directly mediated by CpG methylation in multiple human tumor cells (48). Thus, TET1-mediated DNA hydroxymethylation may be a key player in tumor growth (46).

In summary, our findings demonstrated that EPA-related anti-tumor proliferation (49) was a result of a TET1-dependent DNA demethylation process. EPA conditioning reduced tumor cell proliferation, possibly by counteracting the decrease in 5hmC and TET1 downregulation, associated with HCC progression (31).

Besides EPA, α-linolenic acid, and docosahexaenoic acid, the other well-known n-3 PUFAs were reported to exert beneficial effects on cancer cells and in chronic diseases, such as insulin resistance and cardiovascular disease (50, 51), which are strongly related to abnormal DNA methylation (52, 53). If individual n-3 PUFAs, which are used generally as a mixture, exhibit the same epigenetic action as EPA, then they may also act as demethylating agents. Much work needs to be carried out to test this hypothesis, especially *in vivo* in physiologic and pathologic conditions. Therefore, present results are the potential starting point for assessing the role of EPA at pharmacological doses in clinical trials. More importantly, they pave the way for the study of PUFA-related DNA demethylation in cancer and other diseases with aberrant DNA methylation. 🄵🄹

AUTHOR CONTRIBUTIONS

A. Vecchini designed the research and wrote the manuscript; V. Ceccarelli, S. Ronchetti, L. Cannarile, M. Billi, and A. Vecchini performed the experiments; V. Ceccarelli, F. Grignani, and A. Vecchini analyzed and interpreted the data; V. Valentini and L. Ottini performed bisulfite pyrosequencing; L. Ottini, C. Riccardi, V. N. Talesa, F. Grignani, and A. Vecchini provided financial support; and all authors read and approved the manuscript.

REFERENCES

1. Iurlaro, M., von Meyenn, F., and Reik, W. (2017) DNA methylation homeostasis in human and mouse development. *Curr. Opin. Genet. Dev.* **43**, 101–109
2. Schübeler, D. (2015) Function and information content of DNA methylation. *Nature* **517**, 321–326
3. Esteller, M. (2008) Epigenetics in cancer. *N. Engl. J. Med.* **358**, 1148–1159
4. Calvisi, D. F., Ladu, S., Gorden, A., Farina, M., Lee, J. S., Conner, E. A., Schroeder, I., Factor, V. M., and Thorgeirsson, S. S. (2007) Mechanistic and prognostic significance of aberrant methylation in the molecular pathogenesis of human hepatocellular carcinoma. *J. Clin. Invest.* **117**, 2713–2722
5. Madakashira, B. P., and Sadler, K. C. (2017) DNA methylation, nuclear organization, and cancer. *Front. Genet.* **8**, 76
6. Esteller, M. (2007) Cancer epigenomics: DNA methylomes and histone-modification maps. *Nat. Rev. Genet.* **8**, 286–298
7. Li, K. K., Luo, L. F., Shen, Y., Xu, J., Chen, Z., and Chen, S. J. (2013) DNA methyltransferases in hematologic malignancies. *Semin. Hematol.* **50**, 48–60
8. Glasspool, R. M., Teodoridis, J. M., and Brown, R. (2006) Epigenetics as a mechanism driving polygenic clinical drug resistance. *Br. J. Cancer* **94**, 1087–1092
9. Linnekamp, J. F., Butter, R., Spijker, R., Medema, J. P., and van Laarhoven, H. W. (2017) Clinical and biological effects of demethylating agents on solid tumours - a systematic review. *Cancer Treat. Rev.* **54**, 10–23
10. Rasmussen, K. D., and Helin, K. (2016) Role of TET enzymes in DNA methylation, development, and cancer. *Genes Dev.* **30**, 733–750
11. Branco, M. R., Ficz, G., and Reik, W. (2011) Uncovering the role of 5-hydroxymethylcytosine in the epigenome. *Nat. Rev. Genet.* **13**, 7–13
12. Ficz, G., Branco, M. R., Seisenberger, S., Santos, F., Krueger, F., Hore, T. A., Marques, C. J., Andrews, S., and Reik, W. (2011) Dynamic regulation of 5-hydroxymethylcytosine in mouse ES cells and during differentiation. *Nature* **473**, 398–402
13. Ito, S., Shen, L., Dai, Q., Wu, S. C., Collins, L. B., Swenberg, J. A., He, C., and Zhang, Y. (2011) Tet proteins can convert 5-methylcytosine to 5-formylcytosine and 5-carboxylcytosine. *Science* **333**, 1300–1303
14. Lian, C. G., Xu, Y., Ceol, C., Wu, F., Larson, A., Dresser, K., Xu, W., Tan, L., Hu, Y., Zhan, Q., Lee, C. W., Hu, D., Lian, B. Q., Kleffel, S., Yang, Y., Neiswender, J., Khorasani, A. J., Fang, R., Lezcano, C., Duncan, L. M., Scolyer, R. A., Thompson, J. F., Kakavand, H., Houvras, Y., Zon, L. I., Mihm, M. C., Jr., Kaiser, U. B., Schatton, T., Woda, B. A., Murphy, G. F., and Shi, Y. G. (2012) Loss of 5-hydroxymethylcytosine is an epigenetic hallmark of melanoma. *Cell* **150**, 1135–1146
15. Yang, H., Liu, Y., Bai, F., Zhang, J. Y., Ma, S. H., Liu, J., Xu, Z. D., Zhu, H. G., Ling, Z. Q., Ye, D., Guan, K. L., and Xiong, Y. (2013) Tumor development is associated with decrease of TET gene expression and 5-methylcytosine hydroxylation. *Oncogene* **32**, 663–669
16. Meyer, B. J., Mann, N. J., Lewis, J. L., Milligan, G. C., Sinclair, A. J., and Howe, P. R. (2003) Dietary intakes and food sources of omega-6 and omega-3 polyunsaturated fatty acids. *Lipids* **38**, 391–398
17. Das, U. N. (2006) Essential fatty acids - a review. *Curr. Pharm. Biotechnol.* **7**, 467–482
18. Vaughan, V. C., Hassing, M. R., and Lewandowski, P. A. (2013) Marine polyunsaturated fatty acids and cancer therapy. *Br. J. Cancer* **108**, 486–492
19. Nabavi, S. F., Bilotto, S., Russo, G. L., Orhan, I. E., Habtemariam, S., Daglia, M., Devi, K. P., Loizzo, M. R., Tundis, R., and Nabavi, S. M. (2015) Omega-3 polyunsaturated fatty acids and cancer: lessons learned from clinical trials. *Cancer Metastasis Rev.* **34**, 359–380
20. Wang, W., Zhu, J., Lyu, F., Panigrahy, D., Ferrara, K. W., Hammock, B., and Zhang, G. (2014) ω-3 polyunsaturated fatty acids-derived lipid metabolites on angiogenesis, inflammation and cancer. *Prostaglandins Other Lipid Mediat.* **113-115**, 13–20
21. Yang, P., Chan, D., Felix, E., Cartwright, C., Menter, D. G., Madden, T., Klein, R. D., Fischer, S. M., and Newman, R. A. (2004) Formation and antiproliferative effect of prostaglandin E(3) from eicosapentaenoic acid in human lung cancer cells. *J. Lipid Res.* **45**, 1030–1039
22. Yang, P., Jiang, Y., and Fischer, S. M. (2014) Prostaglandin E3 metabolism and cancer. *Cancer Lett.* **348**, 1–11
23. Ceccarelli, V., Racanicchi, S., Martelli, M. P., Nocentini, G., Fettucciari, K., Riccardi, C., Marconi, P., Di Nardo, P., Grignani, F., Binaglia, L., and Vecchini, A. (2011) Eicosapentaenoic acid demethylates a single CpG that mediates expression of tumor suppressor CCAAT/enhancer-binding protein delta in U937 leukemia cells. *J. Biol. Chem.* **286**, 27092–27102
24. Ceccarelli, V., Nocentini, G., Billi, M., Racanicchi, S., Riccardi, C., Roberti, R., Grignani, F., Binaglia, L., and Vecchini, A. (2014) Eicosapentaenoic acid activates RAS/ERK/C/EBPβ pathway through H-Ras intron 1 CpG island demethylation in U937 leukemia cells. *PLoS One* **9**, e85025
25. Gerashchenko, B. I., Azzam, E. I., and Howell, R. W. (2004) Characterization of cell-cycle progression and growth of WB-F344 normal rat liver epithelial cells following gamma-ray exposure. *Cytometry A* **61**, 134–141
26. Herman, J. G., Graff, J. R., Myöhänen, S., Nelkin, B. D., and Baylin, S. B. (1996) Methylation-specific PCR: a novel PCR assay for methylation status of CpG islands. *Proc. Natl. Acad. Sci. USA* **93**, 9821–9826
27. Tost, J., and Gut, I. G. (2007) DNA methylation analysis by pyrosequencing. *Nat. Protoc.* **2**, 2265–2275
28. Livak, K. J., and Schmittgen, T. D. (2001) Analysis of relative gene expression data using real-time quantitative PCR and the 2(-Delta Delta C(T)) Method. *Methods* **25**, 402–408
29. Abbas, T., and Dutta, A. (2009) p21 in cancer: intricate networks and multiple activities. *Nat. Rev. Cancer* **9**, 400–414
30. Ye, J., Yao, Y., Song, Q., Li, S., Hu, Z., Yu, Y., Hu, C., Da, X., Li, H., Chen, Q., and Wang, Q. K. (2016) Up-regulation of miR-95-3p in hepatocellular carcinoma promotes tumorigenesis by targeting p21 expression. *Sci. Rep.* **6**, 34034
31. Liu, C., Liu, L., Chen, X., Shen, J., Shan, J., Xu, Y., Yang, Z., Wu, L., Xia, F., Bie, P., Cui, Y., Bian, X. W., and Qian, C. (2013) Decrease of 5-hydroxymethylcytosine is associated with progression of hepatocellular carcinoma through downregulation of TET1. *PLoS One* **8**, e62828
32. Chen, M. L., Shen, F., Huang, W., Qi, J. H., Wang, Y., Feng, Y. Q., Liu, S. M., and Yuan, B. F. (2013) Quantification of 5-methylcytosine and 5-hydroxymethylcytosine in genomic DNA from hepatocellular carcinoma tissues by capillary hydrophilic-interaction liquid chromatography/quadrupole TOF mass spectrometry. *Clin. Chem.* **59**, 824–832
33. Booth, M. J., Ost, T. W., Beraldi, D., Bell, N. M., Branco, M. R., Reik, W., and Balasubramanian, S. (2013) Oxidative bisulfite sequencing of 5-methylcytosine and 5-hydroxymethylcytosine. *Nat. Protoc.* **8**, 1841–1851
34. Rawłuszko-Wieczorek, A. A., Siera, A., and Jagodziński, P. P. (2015) TET proteins in cancer: current 'state of the art'. *Crit. Rev. Oncol. Hematol.* **96**, 425–436
35. Tian, Y. P., Zhu, Y. M., Sun, X. H., and Lai, M. D. (2016) Multiple functions of ten-eleven translocation 1 during tumorigenesis. *Chin. Med. J. (Engl.)* **129**, 1744–1751; [Corrigendum: 2646.]
36. Krey, G., Braissant, O., L'Horset, F., Kalkhoven, E., Perroud, M., Parker, M. G., and Wahli, W. (1997) Fatty acids, eicosanoids, and hypolipidemic agents identified as ligands of peroxisome proliferator-activated receptors by coactivator-dependent receptor ligand assay. *Mol. Endocrinol.* **11**, 779–791
37. Fujiki, K., Shinoda, A., Kano, F., Sato, R., Shirahige, K., and Murata, M. (2013) PPARγ-induced PARylation promotes local DNA demethylation by production of 5-hydroxymethylcytosine. *Nat. Commun.* **4**, 2262
38. Gearing, K. L., Göttlicher, M., Teboul, M., Widmark, E., and Gustafsson, J. A. (1993) Interaction of the peroxisome-proliferator-activated receptor and retinoid X receptor. *Proc. Natl. Acad. Sci. USA* **90**, 1440–1444

39. Echeverría, F., Ortiz, M., Valenzuela, R., and Videla, L. A. (2016) Long-chain polyunsaturated fatty acids regulation of PPARs, signaling: relationship to tissue development and aging. *Prostaglandins Leukot. Essent. Fatty Acids* **114**, 28–34

40. Goldstein, J. T., Dobrzyn, A., Clagett-Dame, M., Pike, J. W., and DeLuca, H. F. (2003) Isolation and characterization of unsaturated fatty acids as natural ligands for the retinoid-X receptor. *Arch. Biochem. Biophys.* **420**, 185–193

41. Bachman, M., Uribe-Lewis, S., Yang, X., Williams, M., Murrell, A., and Balasubramanian, S. (2014) 5-Hydroxymethylcytosine is a predominantly stable DNA modification. *Nat. Chem.* **6**, 1049–1055

42. Ito, S., D'Alessio, A. C., Taranova, O. V., Hong, K., Sowers, L. C., and Zhang, Y. (2010) Role of Tet proteins in 5mC to 5hmC conversion, ES-cell self-renewal and inner cell mass specification. *Nature* **466**, 1129–1133

43. Stroud, H., Feng, S., Morey Kinney, S., Pradhan, S., and Jacobsen, S. E. (2011) 5-Hydroxymethylcytosine is associated with enhancers and gene bodies in human embryonic stem cells. *Genome Biol.* **12**, R54

44. Wiehle, L., Raddatz, G., Musch, T., Dawlaty, M. M., Jaenisch, R., Lyko, F., and Breiling, A. (2015) Tet1 and Tet2 protect DNA methylation canyons against hypermethylation. *Mol. Cell. Biol.* **36**, 452–461

45. Isakova, A., Berset, Y., Hatzimanikatis, V., and Deplancke, B. (2016) Quantification of cooperativity in heterodimer-DNA binding improves the accuracy of binding specificity models. *J. Biol. Chem.* **291**, 10293–10306

46. Neri, F., Dettori, D., Incarnato, D., Krepelova, A., Rapelli, S., Maldotti, M., Parlato, C., Paliogiannis, P., and Oliviero, S. (2015) TET1 is a tumour suppressor that inhibits colon cancer growth by derepressing inhibitors of the WNT pathway. *Oncogene* **34**, 4168–4176

47. Sun, M., Song, C. X., Huang, H., Frankenberger, C. A., Sankarasharma, D., Gomes, S., Chen, P., Chen, J., Chada, K. K., He, C., and Rosner, M. R. (2013) HMGA2/TET1/HOXA9 signaling pathway regulates breast cancer growth and metastasis. *Proc. Natl. Acad. Sci. USA* **110**, 9920–9925

48. Li, L., Li, C., Mao, H., Du, Z., Chan, W. Y., Murray, P., Luo, B., Chan, A. T., Mok, T. S., Chan, F. K., Ambinder, R. F., and Tao, Q. (2016) Epigenetic inactivation of the CpG demethylase TET1 as a DNA methylation feedback loop in human cancers. *Sci. Rep.* **6**, 26591; [Corrigendum: 34435.]

49. Calviello, G., Palozza, P., Piccioni, E., Maggiano, N., Frattucci, A., Franceschelli, P., and Bartoli, G. M. (1998) Dietary supplementation with eicosapentaenoic and docosahexaenoic acid inhibits growth of Morris hepatocarcinoma 3924A in rats: effects on proliferation and apoptosis. *Int. J. Cancer* **75**, 699–705

50. Gu, Z., Shan, K., Chen, H., and Chen, Y. Q. (2015) n-3 Poly-unsaturated fatty acids and their role in cancer chemoprevention. *Curr. Pharmacol. Rep.* **1**, 283–294

51. Anderson, B. M., and Ma, D. W. L. (2009) Are all n-3 polyunsaturated fatty acids created equal? *Lipids Health Dis.* **8**, 33–53

52. Bansal, A., and Pinney, S. E. (2017) DNA methylation and its role in the pathogenesis of diabetes. *Pediatr. Diabetes* **18**, 167–177

53. Fernández-Sanlés, A., Sayols-Baixeras, S., Subirana, I., Degano, I. R., and Elosua, R. (2017) Association between DNA methylation and coronary heart disease or other atherosclerotic events: a systematic review. *Atherosclerosis* **263**, 325–333